Indian Journal of Chemistry
Vol. 60A, January 2021, pp. 62-71

A molecular electron density theory study to understand the strain promoted [3+2] cycloaddition reaction of benzyl azide and cyclooctyne

Nivedita Acharjee* & Sourav Mondal
Department of Chemistry, Durgapur Government College, Durgapur 713 214, Paschim Bardhaman, West Bengal, India
*E-mail: nivchem@gmail.com

Received 23 April 2020; revised and accepted 23 October 2020

The strain promoted [3+2] cycloaddition reaction of benzyl azide with cyclooctyne has been studied within the molecular electron density theory (MEDT) at the MPWB1K/6-311G(d,p) computational level. This reaction takes place through a one-step mechanism with activation free energy of 27.1 kcal mol^{-1} in gas phase and 30.2 kcal mol^{-1} in acetonitrile. The activation enthalpies are 13.8 and 16.5 kcal mol^{-1}, respectively in gas phase and acetonitrile. Topological analysis of the electron localization function (ELF) of the reagents shows zwitter-ionic type character of this reaction. The calculated activation free energy is lowered by 5.0 kcal mol^{-1} in gas phase and 4.2 kcal mol^{-1} in acetonitrile relative to the analogues reaction with acetylene. The corresponding activation enthalpy is lowered by 6.4 kcal mol^{-1} in gas phase and 5.9 kcal mol^{-1} in acetonitrile. A comparative bonding evolution theory (BET) analysis of the two reactions reveals lower energy requirements for the depopulation of the alkyne framework and the formation of *pseudoradical* centers along the reaction path of the cyclooctyne reaction. Topological analysis of the ELF and the Quantum Theory of Atoms in Molecules (QTAIM) parameters reveal early transition states with no covalent bonding interactions between the reacting nuclei, which is consistent with the forming bond distances greater than 2 Å in each case.

Keywords: Strain promoted cycloaddition, Electron localization function, Molecular Electron Density Theory

The [3+2] cycloaddition (32CA) reactions[1,2] of azides with cycloalkynes present an important class of chemical transformations due to their simplicity and wide applicability as a clean bioconjugation[3-6] tool in chemical biology and material sciences. These reactions identified in the 1960s by Wittig and Krebs[7] take place simply by mixing and stirring the reactants in a solvent (generally acetonitrile) at room temperature, without the necessity of reagents, catalysts or special reaction conditions. The strain present in cycloalkynes is the underlying synthetic strategy of such reactions, which makes them unique among the azide-alkyne 32CA reactions.

A theoretical analysis is thus worth investigating to obtain a complete comprehension of the reactivity observed in these strain promoted cycloaddition reactions. With the advent of computational chemistry in the last two decades, various theoretical models have been employed to study organic reactions. Balanarayan[8] developed a new algorithm to locate critical points and thus studied the topography of molecular scalar fields, while the electronic reorganisations in cycloaddition reactions were analysed from the electrostatic potential topography in 2007[9]. The quantitative assessment of inductive effect was presented by using molecular electrostatic potential in 2008[10].

The underlying theories to explain organic reactivity in the so called "pericyclic reactions" was primarily based on the 50 years old frontier molecular orbital (FMO) theory in spite of its failure and criticism in several cases[11], until the proposal of molecular electron density theory[12-14] (MEDT) by Domingo in 2016. MEDT establishes the straightforward connection between changes in electron density and chemical reactivity of organic molecules and has been applied successfully to analyse several organic reactions since last 4 years[13,14].

With this in mind, the present study aims to report a comparative theoretical analysis for the reactions of benzyl azide **1** with cyclooctyne **2** and acetylene **3** (Scheme 1) within the molecular electron density theory[12-14] (MEDT) perspective. The MPW functional has been recently stressed as a suitable method for theoretical analysis of [3+2] cycloaddition (32CA) reactions[15] and therefore has been applied in the present investigation. We have recently used this functional in MEDT studies of the 32CA reactions of nitrones, nitrile oxides and azides leading to

isoxazolidines[16], spiroisoxazolines[17,18] and 1,5-disubstituted 1,2,3-triazoles[19].

This theoretical study has been shaped into five sections:

(1) An electron localisation function (ELF) topological analysis of the reactants is carried out. The concept of ELF was first constructed by Becke and Edgecombe in 1990[20] and was further illustrated by Silvi and Savin in 1994[21]. ELF attractor positions are associated with the core nuclei, bonding and non-bonding regions present in a chemical structure and can be classified as core, bonding or non-bonding attractors[21]. Core attractors surround the atomic nuclei, while the bonding attractors are located between the bonding nuclei. The non-bonding attractor positions are associated with the lone pairs, *pseudoradical* centers etc. The non-overlapping partition of the space of an attractor is a basin that can be classified as monosynaptic, disynaptic or polysynaptic in order depending on the participation of one, two or more atomic centers. A monosynaptic basin integrating less than 1 e is associated with *pseudoradical* centre, and integrating 2 e is a carbenoid centre. Domingo[12-14] provided the classification of three atom components (TACs) participating in 32CA reactions from ELF topological analysis. TACs having two *pseudoradical* centers are called *pseudodiradical* type, while TACs having one *pseudoradical* center are called *pseudo(mono)radical* type. TACs with a carbenoid centre are classified as carbenoid type. Finally, TACs which do not have *pseudoradical* or carbenoid centers are classified as zwitter-ionic TACs. Accordingly, the 32CA reactions are classified as *pdr*- type, *pmr*- type, cb- type and zw- type depending on the participation of *pseudodiradical*, *pseudo(mono)radical*, carbenoid and zwitter-ionic TACs respectively. The *pdr-type* 32CA reactions can be carried out very easily while zw-*type* 32CA reactions demand adequate nucleophilic/electrophilic activations to take place[15]. In the present study, ELF of **1**, **2** and **3** was studied to analyse their reactivity in 32CA reactions.

(2) The conceptual density functional theory (CDFT) indices[22,23] at the ground state of the reactants are analysed to obtain an initial comprehension of the polar character of the 32CA reactions.

(3) The transition states (TSs) associated with the 32CA reactions are located and the energy profile is studied. The global electron density transfer[24] (GEDT) at the TSs is calculated to assess the global electronic flux along the reactions.

(4) ELF topological analysis along the reaction paths is compared to structure the molecular mechanism of the 32CA reactions.

(5) Quantum Theory of Atoms in Molecules[25,26] (QTAIM) parameters at the TSs is calculated to assess the nature of bonding at the interatomic bonding regions.

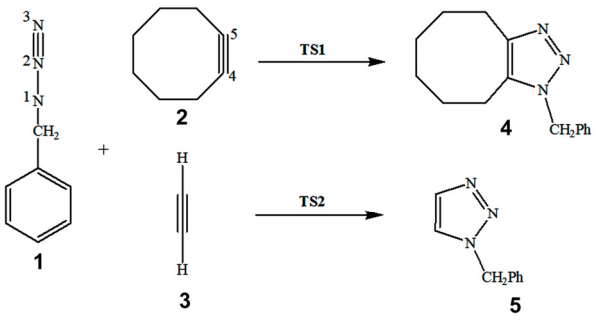

Scheme 1 — 32CA reactions of benzyl azide **1** with cyclooctyne **2** and with acetylene **3**

Materials and Methods

Computational Methods

Optimization of reactants, products and transition states was done using the Berny analytical gradient optimization method[27,28] with the MPWB1K functional[29] in conjunction with the 6-311G(d,p) basis set[30]. All the stationary points were definitely identified for minima with number of imaginary frequencies = 0 or TSs with number of imaginary frequencies = 1. Intrinsic reaction coordinate (IRC) calculations[31-33] were performed to verify that the energy curve connecting the optimized reactants and the products passes through the correct and the lowest TS which must be a first-order saddle point.

The global reactivity indices, electronic chemical potential[34,22,23] μ and chemical hardness[35] η, were calculated from the HOMO (E_{HOMO}) and LUMO (E_{LUMO}) energies using Eqns 1 and 2.

$$\mu \approx (E_{HOMO} + E_{LUMO})/2 \quad \ldots (1)$$

$$\eta \approx E_{LUMO} - E_{HOMO} \quad \ldots (2)$$

The electrophilicity index[36] ω is expressed in terms of the electronic chemical potential μ and chemical hardness η by the Eqn 3:

$$\omega = \mu^2/2\eta \quad \ldots (3)$$

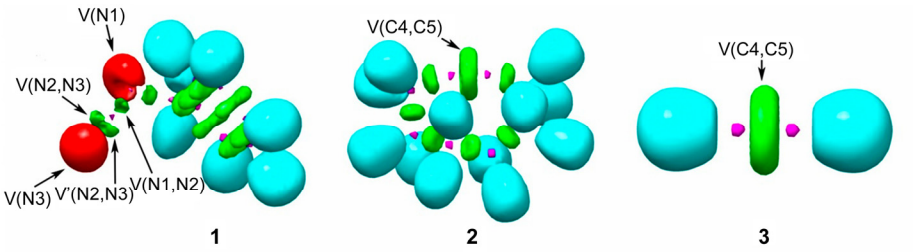

Fig. 1 — MPWB1K/6-311G(d,p) ELF localisation domains represented at an isosurface value of ELF = 0.81 of benzyl azide **1**, cyclooctyne **2**, and acetylene **3.** Protonated basins are shown in blue, disynaptic basins are shown in green, monosynaptic basins are shown in red and core basins are shown in magenta colours

Table 1 — MPWB1K/6-311G(d,p) calculated most significant ELF valence basin populations at benzyl azide **1**, cyclooctyne **2**, and acetylene **3**. ELF valence basin populations are given in average number of electrons, e

	1	2	3
V(N1)	3.53	--	--
V(N1,N2)	2.54	--	--
V(N2,N3)	2.27	--	--
V'(N2,N3)	1.83	--	--
V(N3)	3.76	--	--
V(C4,C5)	--	5.46	5.29

The relative nucleophilicity index[22,37] N is expressed as

$$N = E_{HOMO} - E_{HOMO(tetracyanoethylene)} \quad \ldots (4)$$

The global electron density transfer[24] (GEDT) was calculated from the natural population analysis (NPA[38,39]) as

$$GEDT = \Sigma q_A \quad \ldots (5)$$

where q_A is the net charge and the sum is taken over all the atoms of the nucleophile.

Solvent effects in acetonitrile were taken into account using conductor like polarisable continuum model[40,41] (PCM) in the framework of the self-consistent reaction field[42-44] (SCRF). Enthalpies, entropies and Gibbs free energies were calculated at reaction conditions 298 K (25 °C) and 1 atm.

Topological analysis of the ELF[20,21] and QTAIM[25,26] was performed using Multiwfn[45] software. ELF basin analysis was done with high quality grid with spacing 0.06 Bohr. Basins were visualized using Gauss view software. ELF localization domains were visualized using UCSF Chimera software[46]. All calculations were carried out using Gaussian 2003[47] set of programs along with the graphical interface Gauss View 2003.

Results and Discussion

ELF topological analysis of benzyl azide 1, cyclooctyne 2 and acetylene 3

The electron localization function (ELF[20,21]) establishes a straightforward quantitative connection between the electron density distribution and the chemical structure. The ELF topological analysis of benzyl azide **1** was performed to study its reactivity in 32CA reactions. Additionally, the ELF of cyclooctyne **2** and acetylene **3** was also analyzed. The most significant valence basin populations are listed in Table 1, while the ELF localization domains of the reagents are given in Fig. 1. The natural atomic charges of **1**, **2** and **3** are shown in Fig. 2.

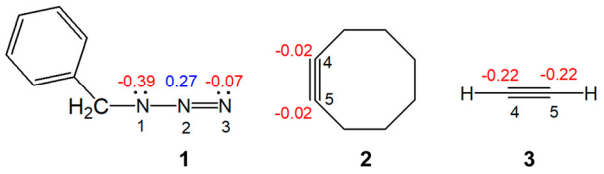

Fig. 2 — MPWB1K/6-311G(d,p) calculated natural atomic charges, in average number of electrons e, of benzyl azide **1**, cyclooctyne **2** and acetylene **3**. Negative charges are coloured in red, and positive charges in blue

ELF topology of benzyl azide **1** shows the presence of two monosynaptic basins, V(N1) and V(N3), integrating 3.53 and 3.76 e, respectively, a V(N1,N2) disynaptic basin integrating 2.54 e, and a pair of disynaptic basins, V(N2,N3) and V'(N2,N3), integrating population of 2.27 e and 1.83 e. The V(N1) and V(N3) monosynaptic basins can be associated with the non-bonding electron density on the N1 and N3 nitrogen, respectively. The pair of V(N2,N3) and V'(N2,N3) disynaptic basins can be associated with the N2–N3 double bond, while V(N1,N2) disynaptic basin is associated with underpopulated N1–N2 double bond. Thus, benzyl azide **1** can be classified as zwitter-ionic (*zw*-) type TAC[15] owing to the absence of *pseudoradical* or carbenoid centers.

ELF of cyclooctyne **2** and acetylene **3** shows the presence of one V(C4,C5) disynaptic basins integrating a total of 5.46 and 5.29 e, respectively, which can be associated with underpopulated C-C triple bond.

In benzyl azide **1**, the N1 nitrogen is negatively charged by –0.39 e, the N2 nitrogen is positively charged by 0.27 e, and the terminal N3 nitrogen shows a negligible charge of –0.07 e. This charge distribution does not follow the commonly accepted zwitterionic structure of azides, where the negative charge should be concentrated at the terminal N3 nitrogen. Cyclooctyne **2** and acetylene **3** both show negative charges at C4 and C5 carbons, with the higher calculated value for acetylene.

Analysis of the global and local reactivity indices of the reactants

Conceptual density functional theory[22,23] (CDFT) is a powerful tool to the understanding of the reactivity of molecules, especially for 32CA reactions. The standard electrophilicity[36] and nucleophilicity[37] scales are defined at B3LYP/6-31G(d) computational level, which has also been used for the present study. The electronic chemical potential, μ, chemical hardness, η, electrophilicity, ω, and nucleophilicity, N, at the ground state of benzyl azide **1**, cyclooctyne **2**, and acetylene **3** are listed in Table 2.

The electronic chemical potential[22,23] of benzyl azide **1**, μ = –3.74 eV, is slightly lower than those of that of acetylene **3**, μ = –3.11 eV, indicating that the corresponding 32CA reactions will have low polar character. However, cyclooctyne **2** shows higher μ value (μ = –2.69 eV) than benzyl azide **1**, thus suggesting some polar character for the 32CA reaction.

The electrophilicity[36] ω and nucleophilicity[37] N indices of benzyl azide **1** are 1.19 and 2.42 eV respectively, being classified a moderate electrophile and moderate nucleophile within the corresponding scales. Cyclooctyne **2** and acetylene **3** are classified as marginal electrophiles, ω < 0.80 eV, while they differ in the nucleophilicity classification. Cyclooctyne **2** is classified as moderate nucleophile (2.00 eV < N < 3.00 eV), while acetylene **3** as marginal nucleophile (N < 2.00 eV).

Analysis of the energy profile associated with the 32CA reactions of benzyl azide 1 with cyclooctyne 2 and with acetylene 3

Due to the molecular symmetry of cyclooctyne **2** and acetylene **3**, only one reaction path is feasible for their 32CA reactions with benzyl azide **1**. The search for the stationary points involved in the reaction paths associated to these 32CA reactions allowed characterising the reactants, **1**, **2**, **3**, one TS for each 32CA reaction, **TS1** & **TS2**, and the corresponding 1,2,3-triazoles, **4** and **5**, respectively, (Scheme 1). The relative energies and thermodynamic data of TSs and 1,2,3-triazoles are given in Table 3, while the total values are given in Supplementary Data.

The activation enthalpies associated with these 32CA reactions are 13.8 (**TS1**), and 20.2 (**TS2**) kcal·mol^{-1} in gas phase, and 16.5 (**TS1**) and 22.4 (**TS2**) kcal·mol^{-1} in acetonitrile at 298 K and 1 atm; the reactions being strongly exothermic with reaction enthalpies of –86.5 and –77.1 kcal·mol^{-1} in gas phase, and –88.0 and –78.3 kcal·mol^{-1} in acetonitrile. Analysis of the relative enthalpies allows establishing some appealing conclusions: (i) Activation enthalpy of the zw-*type* 32CA reaction between benzyl azide **1** and cyclooctyne **2** *via* **TS1** is lowered than the 32CA reaction between benzyl azide **1** and acetylene **3** by 6.4 kcal·mol^{-1} in gas phase, and by 5.9 kcal·mol^{-1} in acetonitrile. Consequently, a strong acceleration of the zw-*type* 32CA reaction of benzyl azide **1** involving cyclooctyne **2** is found compared to 32CA reactions of azides with simple alkynes. This is in complete agreement with the experimental findings[1]. (ii) The reaction enthalpy of the zw-*type* 32CA reaction between benzyl azide **1** and cyclooctyne **2** is lowered than the 32CA reaction between benzyl azide **1** and acetylene **3** by 9.4 kcal·mol^{-1} in gas phase, and by 9.7 kcal·mol^{-1} in acetonitrile. The strong exothermic character of these 32CA reactions makes the reactions irreversible. (iii) The inclusion of solvent effects of acetonitrile increases the activation enthalpies by

Table 2 — B3LYP/6-31G(d) calculated electronic chemical potential μ, chemical hardness η, global electrophilicity ω and global nucleophilicity N, in eV, of benzyl azide **1**, cyclooctyne **2** and acetylene **3**

	μ	η	ω	N
1	–3.74	5.90	1.19	2.42
2	–2.69	7.40	0.49	2.72
3	–3.11	9.06	0.54	1.47

Table 3 — MPWB1K/6-311G(d,p) calculated relative energies, enthalpies and Gibbs free energies, in kcal·mol^{-1}, computed at 298K of the stationary points involved in the 32CA reactions of benzyl azide **1** with cyclooctyne **2** and with acetylene **3**

	ΔE	ΔH	ΔG
TS1 (gas phase)	13.7	13.8	27.1
4 (gas phase)	–90.1	–86.5	–69.5
TS1 (acetonitrile)	16.2	16.5	30.2
4 (acetonitrile)	–91.9	–88.0	–70.8
TS2 (gas phase)	20.1	20.2	32.1
5 (gas phase)	–81.4	–77.1	–64.2
TS2 (acetonitrile)	22.2	22.4	34.4
5 (acetonitrile)	–82.8	–78.3	–65.3

2.7 and 2.2 kcal·mol^{-1}, while the reaction enthalpies are increased by 1.5 and 1.2 kcal·mol^{-1}. (iv) The inclusion of entropies to enthalpies arises the activation Gibbs free energies between 11.9 and 13.7 kcal·mol^{-1} and decreases the exergonic character of these reactions between 12.9 and 17.2 kcal·mol^{-1} because of the bimolecular character of these 32CA reactions.

The MPWB1K/6-311G(d,p) optimised geometry of TSs are given in Fig. 3. In gas phase, the distances between N1 and C5, and N3 and C4 interacting centres at the four TSs are: 2.186 and 2.166 Å at **TS1** (gas phase), 2.197 and 2.177 Å at **TS1** (acetonitrile)**,** 2.107 and 2.140 Å at **TS2** (gas phase) and 2.108 and 2.150 Å at **TS2** (acetonitrile), respectively. These geometrical parameters indicate that **TS1** is associated with lower asynchronous processes with the N3–C4 distances shorter than the N1–C5 ones, while at **TS2**, a slight increased asynchronicity is observed with the N1–C5 distances shorter than the N3–C4 forming single bond.

Finally, in order to evaluate the polar nature of these 32CA reactions, the GEDT[24] at the TSs was analyzed. The GEDT values at the TSs are 0.010 e at **TS1** and 0.004 e at **TS2**. Increase in GEDT for 32CA reaction of cyclooctyne **2** compared to acetylene **3** is consistent with the increased electronic chemical potential of cyclooctyne **2** (Table 2).

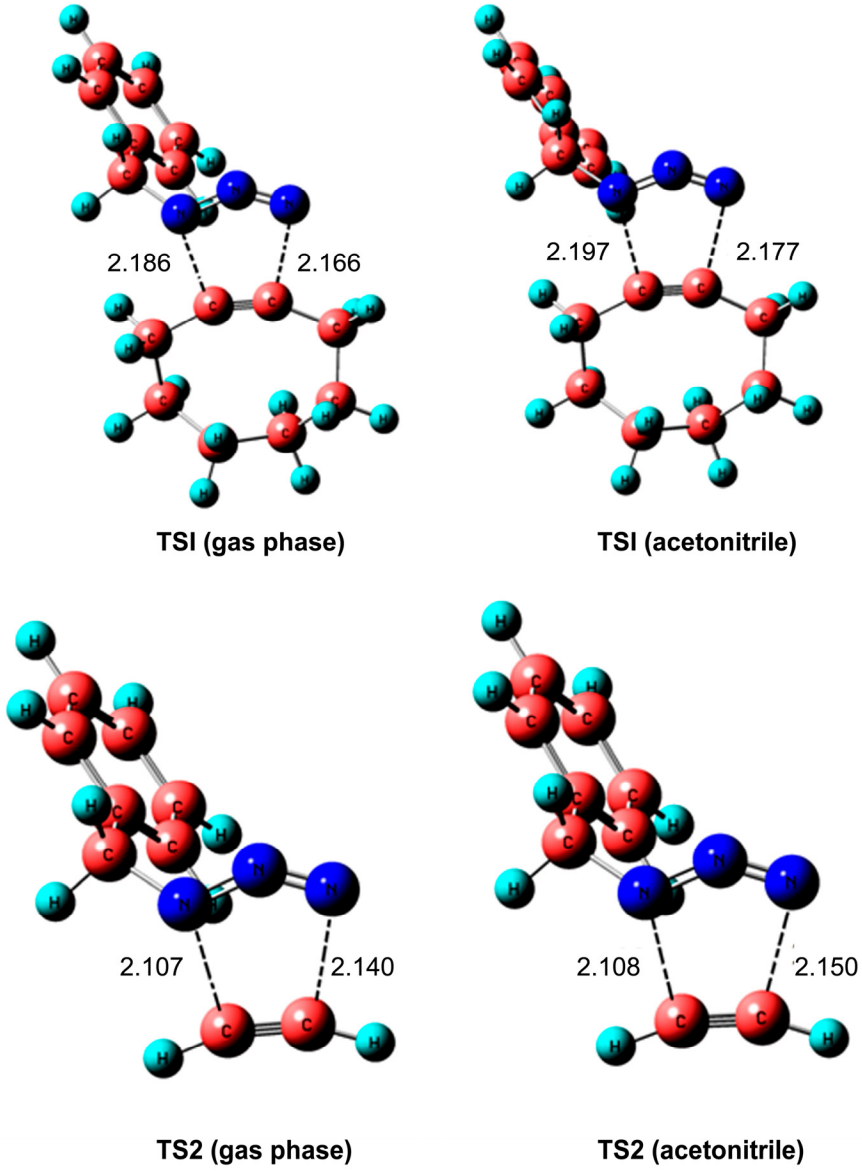

Fig. 3 — MPWB1K/6-311G(d,p) optimised geometries of the TSs involved in the 32CA reactions of benzyl azide **1** with cyclooctyne **2** and acetylene **3**. Bond lengths are in Angstrom

ELF topological analysis of the reaction paths for the 32CA reactions of benzyl azide 1 with cyclooctyne 2 and with acetylene 3

The Bonding evolution theory (BET)[48] proposed by Krokoidis in 1997, comes from the conjunction of ELF topological analysis[20,21] and Thom's Catastrophe theory[49]. It has proven to be a very useful methodological tool to establish the nature of the electronic rearrangement associated along the reaction path. Herein, a comparative study of the BETs of the 32CA reactions of benzyl azide **1** with cyclooctyne **2** and with acetylene **3** is presented. The 32CA reactions of **1** with **2** and **3** take place along nine different phases (Table 4 and Table 5).

Phase I starts at **P0-I** for the **1/2** reaction system, d_{N3-C4} = 2.96 Å and d_{N1-C5} = 2.76 Å and at **P0-II** for the **1/3** reaction system, d_{N3-C4} = 3.03 Å and d_{N1-C5} =

Table 4 — ELF valence basin populations, distances of the forming bonds, and relative[a] electronic energies of the IRC structures **P0-I** – **P8-I** defining the nine phases characterizing the molecular mechanism of the 32CA reaction between **1** with **2** yielding cycloadduct **4.** Distances are given in angstroms, Å, and relative energies in kcal·mol^{-1}

Phases	*I*	*II*	*III*	*IV*	*V*	*VI*	*VII*	*VIII*	*IX*	
Structures	**P0-I**	**P1-I**	**P2-I**	**P3-I**	**P4-I**	**P5-I**	**P6-I**	**P7-I**	**P8-I**	**4**
d(N3–C4)	2.964	2.798	2.566	2.334	2.166	1.952	1.876	1.741	1.585	1.346
d(N1–C5)	2.761	2.646	2.477	2.310	2.186	2.015	1.951	1.833	1.683	1.346
ΔE	0.0	2.6	6.6	11.7	13.7	7.8	2.2	-12.4	-35.1	-90.1
V(N1)	3.46	3.44	3.41	3.42	3.43	2.28	2.13	1.99	1.85	0.67
V'(N1)						1.16	1.32	1.77		
V(N2)			0.57	1.54	2.00	2.36	2.46	2.61	2.76	3.15
V(N1,N2)	2.55	2.53	2.38	2.05	1.86	1.77	1.75	1.75	1.74	1.77
V(N2,N3)	1.66	4.16	3.76	3.14	2.91	2.69	2.62	2.51	2.38	2.04
V'(N2,N3)	2.47									
V(N3)	3.75	3.75	3.73	3.71	3.73	3.81	3.45	3.24	3.10	2.90
V′(N3)							0.39			
V(C4,C5)	5.41	5.41	5.39	2.66	2.54	2.26	2.19	2.09	2.02	3.43
V'(C4,C5)				2.67	2.48	2.28	2.19	2.07	1.96	
V(C4)					0.27	0.61	0.67			
V(C5)						0.16	0.24			
V(N3,C4)								1.42	1.70	2.32
V(N1,C5)									1.96	2.97

Table 5 — ELF valence basin populations, distances of the forming bonds, and relative[a] electronic energies of the IRC structures **P0-II** – **P8-II** defining the nine phases characterizing the molecular mechanism of the 32CA reaction between **1** with **3** yielding cycloadduct **5**. Distances are given in angstroms, Å, and relative energies in kcal·mol^{-1}

Phases	*I*	*II*	*III*	*IV*	*V*	*VI*	*VII*	*VIII*	*IX*	
Structures	**P0-II**	**P1-II**	**P2-II**	**P3-II**	**P4-II**	**P5-II**	**P6-II**	**P7-II**	**P8-II**	**5**
d(N3–C4)	3.032	2.833	2.562	2.103	1.999	1.970	1.882	1.721	1.678	1.346
d(N1–C5)	2.841	2.692	2.462	2.075	1.985	1.958	1.878	1.729	1.687	1.341
ΔE	0.0	2.8	8.7	19.9	16.5	14.6	6.5	–16.3	–23.8	–81.4
V(N1)	3.47	3.43	3.41	3.42	3.41	2.20	2.05	1.89	1.85	0.66
V'(N1)						1.20	1.63	1.87		
V(N2)			0.52	2.11	2.29	2.34	2.46	2.65	2.69	3.11
V(N1,N2)	2.55	2.55	2.39	1.81	1.77	1.76	1.75	1.75	1.75	1.79
V(N2,N3)	2.41	4.13	3.78	2.85	2.74	2.71	2.63	2.49	2.45	2.05
V'(N2,N3)	1.70									
V(N3)	3.77	3.77	3.74	3.73	3.76	3.77	3.46	3.22	3.17	2.89
V′(N3)							0.35			
V(C4,C5)	2.15	2.17	2.35	2.45	2.24	2.20	2.08	1.95	1.93	3.34
V'(C4,C5)	3.10	3.08	1.81	2.38	2.23	2.18	2.06	1.93	1.90	
V"(C4,C5)			1.09							
V(C4)				0.23	0.50	0.56	0.68			
V(C5)					0.12	0.18				
V(N3,C4)								1.46	1.54	2.27
V(N1,C5)									1.92	2.91

2.84 Å which corresponds with the first structures of the respective IRCs. ELF of **P0-I** and **P0-II** is similar to that of the separated reagents (see section 3.1).

The short phase *Phase II* starts at **P1-I** for the **1/2** reaction system, d_{N3-C4} = 2.80 Å and d_{N1-C5} = 2.65 Å and at **P1-II** for the **1/3** reaction system, d_{N3-C4} = 2.83 Å and d_{N1-C5} = 2.69 Å with the respective energy cost (EC) of 2.6 and 2.8 kcal·mol^{-1}. The two V(N2,N3) and V'(N2,N3) disynaptic basins present at **P0-I** and **P0-II** have merged into a new V(N2,N3) disynaptic basin, respectively integrating at 4.16 e and 4.13 e.

Phase III starts at **P2-I** for the **1/2** reaction system, d_{N3-C4} = 2.57 Å and d_{N1-C5} = 2.48 Å and at **P1-II** for the **1/3** reaction system, d_{N3-C4} = 2.56 Å and d_{N1-C5} = 2.46 Å with the respective energy cost (EC) of 6.6 and 8.7 kcal·mol^{-1}. This phase is characterised by the creation of monosynaptic V(N2) basin associated with the lone pair at N2 nitrogen. The electron density of this lone pair mainly comes from the depopulation of the N1-N2 and N2-N3 bonding regions along *Phase III* and requires higher EC in case of **1**/**3** reaction system.

For the **1**/**2** reaction system, *Phase IV* starts at **P3-I**, d_{N3-C4} = 2.33 Å and d_{N1-C5} = 2.31 Å with energy cost of 11.7 kcal·mol^{-1}.The disynaptic V(C4,C5) disynaptic basins present at **P0-I** has split into a two disynaptic basins V(C4,C5) and V'(C4,C5), respectively integrating at 2.66 e and 2.67 e .

Phase V starts at **P4-I** for the **1/2** reaction system, d_{N3-C4} = 2.17 Å and d_{N1-C5} = 2.19 Å and *Phase IV* starts at **P3-II** for the **1/3** reaction system, d_{N3-C4} = 2.10 Å and d_{N1-C5} = 2.08 Å with the respective energy cost (EC) of 11.7 and 19.9 kcal·mol^{-1}. These phases are characterised with the creation of V(C4) monosynaptic basin, respectively integrating at 0.27 e and 0.23 e. This monosynaptic basin is associated with the formation of *pseudoradical* centre at C4. The electron density of this lone pair mainly comes from the depopulation of the C4-C5 bonding region.

Phase VI starts at **P5-I** for the **1/2** reaction system, d_{N3-C4} = 1.95 Å and d_{N1-C5} = 2.02 Å and *Phase V* starts at **P4-II** for the **1/3** reaction system, d_{N3-C4} = 1.99 Å and d_{N1-C5} = 1.99 Å. **P5-I and P4-II** are characterised by the creation of a new V(C5) monosynaptic basin, respectively integrating 0.16 e and 0.12 e, associated with the formation of a *pseudoradical* center at the C5 carbon. Together with this change, at **P5-I**, the V(N1) monosynaptic basin splits into two basins integrating 2.28 e and 1.16 e. For the **1/3** system splitting of the monosynaptic V(N1) basin into two monosynaptic basins V(N1) and V'(N1) integrating 2.20 e and 1.20 e is observed in *Phase VI* starting at **P5-II**, d_{N3-C4} = 1.97 Å and d_{N1-C5} = 1.96 Å.

Phase VII starts at **P6-I** for the **1/2** reaction system, d_{N3-C4} = 1.88 Å and d_{N1-C5} = 1.95 Å and at **P6-II** for the **1/3** reaction system, d_{N3-C4} = 1.88 Å and d_{N1-C5} = 1.88 Å. In this phase, the V(N3) monosynaptic basin present at **P5-I** and **P5-II** splits into two V(N3) and V'(N3) monosynaptic basins.

Phase VIII starts at **P7-I** for the **1/2** reaction system, d_{N3-C4} = 1.74 Å and d_{N1-C5} = 1.83 Å and at **P7-II** for the **1/3** reaction system, d_{N3-C4} = 1.72 Å and d_{N1-C5} = 1.73 Å. At the beginning of this phase the first more relevant change along the IRCs takes place. At this structure, while the V(C4) and V'(N3) monosynaptic basin present at **P7-I** and **P7-II** are missing, a new V(N4,C3) disynaptic basin, respectively integrating 1.42 e and 1.46 e, is created. This topological change indicates that the formation of the first N3–C4 single bond has begun at a C–N distance of 1.7 Å.

Finally, the last *Phase XI* starts at **P8-I** for the **1/2** reaction system, d_{N3-C4} = 1.59 Å and d_{N1-C5} = 1.68 Å and at **P8-II** for the **1/3** reaction system, d_{N3-C4} = 1.68 Å and d_{N1-C5} = 1.69 Å. At **P8-I** and **P8-II**, the second more relevant change along the IRC takes place. At these structures, while the V(C5) and V'(N1) monosynaptic basins are missing, a new V(N1,C5) disynaptic basin, integrating 1.96 e and 1.92 e, is created. These relevant topological changes indicate that the formation of the second N1-C5 single bond has begun, through the C- to -N coupling of the electron density of the C5 *pseudoradical* carbon and part of the non-bonding electron density of the N1 nitrogen. Along this last phase, the molecular electron density is relaxed to reach the structure of cycloadducts **4** and **5** in the 32CA reactions, in which the population of the V(N3,C4) and V(N1,C5) disynaptic basins reach a population of 2.32 e (**4**) & 2.27 e (**5**) and 2.97 e (**4**) & 2.91 e (**5**), respectively (Table 4 and Table 5).

ELF topological analysis at the TSs

The ELF topology of the four TSs were analysed and compared. The populations of the most significant ELF valence basin at the TSs are given in Table 6, while the ELF localization domains are shown in Fig. 4.

ELF of the TSs shows the presence of two monosynaptic basins, V(N1) and V(N3), which are associated with the non-bonding electron densities at

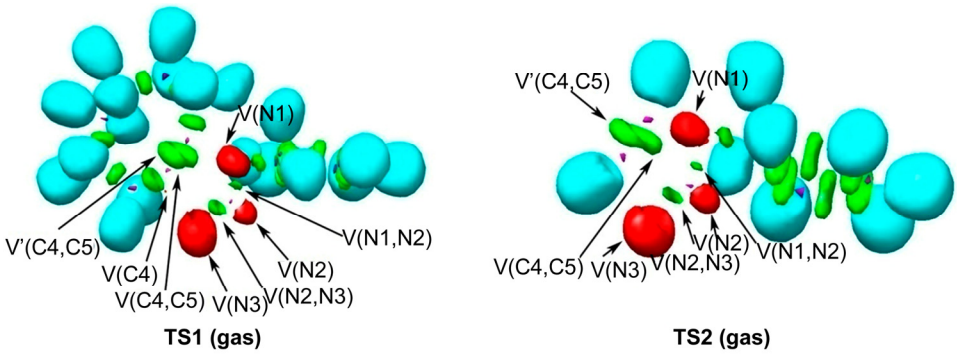

Fig. 4 — MPWB1K/6-311G(d,p) ELF localisation domains of the TSs associated with the 32CA reactions of **1** with **2** and **3**

Table 6 — MPWB1K/6-311G(d,p) calculated most significant ELF valence basin populations at the four TSs

	TS1 (gas phase)	**TS1** (acetonitrile)	**TS2** (gas phase)	**TS2** (acetonitrile)
V(N1)	3.43	3.40	3.42	3.38
V(N1, N2)	1.86	1.88	1.84	1.86
V(N2, N3)	2.90	2.88	2.89	2.85
V(N2)	2.00	1.99	2.04	2.03
V(N3)	3.73	3.78	3.72	3.78
V(C4, C5)	2.48	2.51	2.42	2.43
V'(C4 ,C5)	2.54	2.50	2.66	2.61
V(C4)	0.27	0.26	--	--

Table 7 — QTAIM parameters, in au, of (3,-1) CPs at the TSs in the regions associated with formation of new N3–C4 (**CP1**) and N1–C5 (**CP2**) single bonds

	CP1 (N3–C4)			**CP2** (N1–C5)		
	ρ	$\nabla^2_{\rho(r_c)}$	$E_{\rho(r_c)}$	ρ	$\nabla^2_{\rho(r_c)}$	$E_{\rho(r_c)}$
TS1 (gas)	0.056	0.098	–0.007	0.055	0.099	–0.007
TS1 (acetonitrile)	0.055	0.096	–0.006	0.053	0.098	–0.006
TS2 (gas)	0.059	0.100	–0.008	0.063	0.107	–0.010
TS2 (acetonitrile)	0.058	0.099	–0.007	0.063	0.107	–0.010

the N1 and N3 nitrogen, already present in benzyl azide **1** (Table 1 and Table 6). ELF of the TSs also shows the presence of one V(N2) monosynaptic basin, integrating 1.99 - 2.04 e, whose electron density comes from the depopulation of the N1–N2 and N2–N3 bonding regions. Note that V(N1,N2) disynaptic basin experiences a depopulation of the electron density from 3.53 e in **1** to 3.43 in **TS1** and to 3.42 in **TS2**, respectively, while the N2–N3 bonding region experiences a depopulation of the electron density from 4.10 e in **1** to 2.90 in **TS1** and to 2.89 e in **TS2**, respectively.

At the alkyne framework, a pair of disynaptic basins, V(C4,C5) and V'(C4,C5), associated with C4–C5 bonding region integrating a total population of 5.02 e (**TS1**) and 5.08 e (**TS2**) is observed, which indicates a depopulation of 0.44 e and 0.38 e, respectively relative to the reagents. ELF of **TS1** shows the presence of one V(C4) monosynaptic basin integrating at 0.27 e, respectively, which is not observed in **TS2**.

Finally, the absence of neither V(N1,C5) nor V(N3,C4) disynaptic basin at these TSs indicates that the formation of new N1–C5 and N3–C4 single bonds has not yet begun, which is consistent with the corresponding N3–C4 and N1–C5 distance above 2.0 Å (Fig. 3).

Topological analysis of the AIM at the TSs

A Quantum Theory of Atoms in Molecules[25,26] (QTAIM) topological analysis of the electron density ρ at the critical points (CPs) corresponding to the molecular region associated with the formation of new N3–C4 and N1–C5 single bonds at the TSs was carried out. The calculated QTAIM parameters are given in Table 7.

Laplacian of electron density $\nabla^2\rho(r_c)$ at **CP1** and **CP2** shows positive values at the TSs. The low electron density $\rho(\mathbf{r_c})$ values together with the positive Laplacian $\nabla^2\rho(r_c)$ at these CPs indicate the absence of any covalent bonding interaction between the carbon and nitrogen nuclei at these TSs, and consequently, that the formation of the new N3–C4 and N1–C5 single covalent bonds has not yet started at these early TSs, in complete agreement with the ELF topological analysis.

Additionally, note that the calculated QTAIM parameters show very small changes between the gas phase values and their acetonitrile counterparts. Solvent calculations are modelled using the United Atom Topological Model within conductor like polarisable continuum model[40,41] (PCM) in acetonitrile within the framework of the self-

consistent reaction field[42]. The optimised geometries of the TSs show variations in gas phase and acetonitrile (Fig. 3), suggesting slight difference in the changes of electron density along the reaction path in acetonitrile relative to the gas phase for both the 32CA reactions. Consequently, the accumulation of electron density at the interatomic bonding regions in the TSs vary in gas phase and acetonitrile, resulting in small changes of the QTAIM parameters at the respective TSs in acetonitrile relative to the gas phase.

Conclusions

The strain promoted cycloaddition reaction of benzyl azide **1** with cyclooctyne **2** has been studied within molecular electron density theory at the MPWB1K/6-311G(d,p) computational level, and compared with the 32CA reaction of the benzyl azide **1** with non-strained acetylene **3**. Topological analysis of benzyl azide **1** allows its classification as zwitterionic TAC participating in zw-*type* 32CA reactions. Analysis of the CDFT indices shows higher polar character for the 32CA reaction of cyclooctyne **2** compared to acetylene **3**, which is also confirmed from the calculated GEDT at the located TSs. The 32CA reactions of benzyl azide **1** with cyclooctyne **2** and acetylene **3** take place through a one-step mechanism. The lowest activation enthalpy corresponds to the 32CA reaction with cyclooctyne **2**, which shows reduction in gas phase of 6.4 kcal·mol^{-1} and in acetonitrile of 5.9 kcal·mol^{-1} relative to that with acetylene **3**. This acceleration of the reaction for cyclooctyne is attributed to the lower energy cost for the depopulation of the alkyne moiety to generate *pseudoradical* centers, which is revealed from a comparative topological analysis of the electron localisation function along the reaction paths. ELF and QTAIM studies show early TSs with no covalent bonding between the reacting nuclei for these 32CA reactions.

Supplementary Data

Supplementary Data associated with this article are available in the electronic form at http://www.nopr.niscair.res.in/jinfo/ijca/IJCA_60A(01)62-71_SupplData.pdf.

Acknowledgement

The authors acknowledge the help and support of Professor Luis R Domingo, Professor, University of Valencia, Spain, for important clarifications in several studies related to the concept of 32CA reactions.

References

1 Dommerholt J, Rutjes F P J T & van Delft F L, *Topp Curr Chem (Z)*, 374 (2016) 16.
2 Huisgen R, *Angew Chem Int Ed Engl*, 2 (1963) 565.
3 Kiick K L, Saxon E, Tirrell D A & Bertozzi C R, *Proc Natl Acad Sci USA*, 99 (2002) 19.
4 Wang Q, Chan T R, Hilgraf R, Fokin V V, Sharpless K B & Finn M G, *J Am Chem Soc*, 125 (2003) 3192.
5 Mbua N E, Guo J, Wolfert M A, Steet R & Boons G J, *ChemBioChem*, 12 (2011) 1912.
6 Singh S, Davidchik I S D & Kluger R, *Org Biomol Chem*, 14 (2016) 10011.
7 Wittig G & Krebs A, *Chem Ber*, 94 (1961) 3260.
8 Balanarayan P & Gadre S R, *J Chem Phys*, 119 (2003) 5037.
9 Balanarayan P, Kavathekar R & Gadre S R, *J Phys Chem A*, 111 (2007) 2733.
10 Suresh C H, Alexander P, Vijayalakshmi K P, Sajith P K & Gadre S R, *Phys Chem Chem Phys*, 10 (2008) 6492.
11 Dewar M J S, *J Mol Struct (Theochem)* 200 (1989) 301.
12 Domingo L R, *Molecules*, 21 (2016) 1319.
13 Gutiérrez M R & Domingo L R, *Eur J Org Chem,* (2019) 267.
14 Domingo L R & Acharjee N, *Frontiers in Computational Chemistry*, Vol 5, Haq Z Q & Wilson A K, Ed (Bentham and Science, Singapore) 2020, p. 174.
15 Domingo L R, Gutiérrez M R & Pérez P, *J Org Chem*, 83 (2018) 2182.
16 Domingo L R & Acharjee N, *Chem Select*, 3 (2018) 8373.
17 Domingo L R, Gutiérrez M R & Acharjee N, *Molecules,* 24 (2019) 832.
18 Acharjee N, *J Mol Model*, 26 (2020) 117.
19 Domingo L R & Acharjee N, *J Phys Org Chem*, 33 (2020) e4062.
20 Becke A D & Edgecombe K E, *J Chem Phys*, 92 (1990) 5397.
21 Silvi B & Savin A, *Nature*, 371 (1994) 683.
22 Geerlings P, De Proft F & Langenaeker W, *Chem Rev*, 103 (2003) 1793.
23 Domingo L R, Gutiérrez M R & Pérez P, *Molecules,* 21 (2016) 748.
24 Domingo L R, *RSC Adv*, 4 (2014) 32415.
25 Bader R F W & Essén H, *J Chem Phys*, 80 (1984) 1943.
26 Bader R F W, *Atoms in Molecules: A Quantum Theory* (Oxford, Clarendon Press, New York) 1990.
27 Schlegel H B, *J Comput Chem*, 2 (1982) 214.
28 Schlegel H B, *Modern Electronic Structure Theory*, Yarkony D R, Ed (World Scientific Publishing, Singapore) 1994.
29 Zhao Y & Truhlar D G, *J Phys Chem A*, 108 (2004) 6908.
30 Hehre W J, Radom L, Schleyer P v R & Pople J A, *Ab initio Molecular Orbital Theory*, (Wiley, New York) 1986.
31 Fukui K, *J Phys Chem*, 74 (1970) 4161.
32 Gonzalez C & Schlegel H B, *J Phys Chem*, 94 (1990) 5523.
33 Gonzalez C & Schlegel H B, *J Chem Phys*, 95 (1991) 5853.
34 Parr R G & W Yang, *Density Functional Theory of Atoms and Molecules*, (Oxford University Press, New York) 1989.
35 Parr R G & Pearson R G, *J Am Chem Soc*, 105 (1983) 7512.
36 Domingo L R, Aurell M J, Pérez P & Contreras R, *Tetrahedron Lett*, 58 (2002) 4417.
37 Domingo L R, Chamorro E & Pérez P, *J Org Chem*, 73 (2008) 4615.
38 Reed A E, Weinstock R B & Weinhold F, *J Chem Phys*, 83 (1985) 735.

39 Reed A E, Curtiss L A & Weinhold F, *Chem Rev*, 88 (1988) 899.

40 Tomasi J & Persico M, *Chem Rev*, 94 (1994) 2027.

41 Simkin B Y & Sheikhet I, *Quantum Chemical and Statistical Theory of Solutions-A Computational Approach,* (Ellis Horwood, London) 1995.

42 Cances E, Mennucci B & Tomasi J, *J Chem Phys*, 107 (1997) 3032.

43 Cossi M, Barone V, Cammi R & Tomasi J, *Chem Phys Lett*, 255 (1996) 327.

44 Barone V, Cossi M & Tomasi J, *J Comput Chem*, 19 (1998) 404.

45 Lu T & Chen F, *J Comp Chem*, 33 (2012) 580.

46 Pettersen E F, Goddard T D, Huang C C, Couch G S, Greenblatt D M, Meng E C, & Ferrin T E, *J Comput Chem*, 25 (2004) 1605.

47 Frisch M J, Trucks G W, Schlegel H B, Scuseria G E, Robb M A, Cheeseman J R, Montgomery Jr J A, Vreven T, Kudin K N, Burant J C, Millam J M, Iyengar S S, Tomasi J, Barone V, Mennucci B, Cossi M, Scalmani G, Rega N, Petersson GA, Nakatsuji H, Hada M, Ehara M, Toyota K, Fukuda R, Hasegawa J, Ishida M, Nakajima T, Honda Y, Kitao O, Nakai H, Klene M, Li X, Knox J E, Hratchian H P, Cross J B, Bakken V, Adamo C, Jaramillo J, Gomperts R, Stratmann R E, Yazyev O, Austin A J, Cammi R, Pomelli C, Ochterski J W, Ayala P Y, Morokuma K, Voth G A, Salvador P, Dannenberg J J, Zakrzewski V G, Dapprich S, Daniels A D, Strain M C, Farkas O, Malick D K, Rabuck A D, Raghavachari K, Foresman J B, Ortiz J V, Cui Q, Baboul A G, Clifford S, Cioslowski J, Stefanov B B, Liu G, Liashenko A, Piskorz P, Komaromi I, Martin R L, Fox D J, Keith T, Al-Laham MA, Peng CY; Nanayakkara A, Challacombe M, Gill P M W, Johnson B, Chen W, Wong M W, Gonzalez C & Pople J A, *Gaussian 03, Rev D.01,* Gaussian, Inc, Wallingford CT, 2004.

48 Krokidis X, Noury S & Silvi B, *J Phys Chem A*, 101 (1997) 7277.

49 Thom R. *Stabilité Structurelle et Morphogénèse*, (Intereditions, Paris) 1972.